Drift-wave eigenmodes in toroidal plasmas

Liu Chen, and C. Z. Cheng

Citation: The Physics of Fluids **23**, 2242 (1980); doi: 10.1063/1.862907
View online: https://doi.org/10.1063/1.862907
View Table of Contents: https://aip.scitation.org/toc/pfl/23/11
Published by the American Institute of Physics

Drift-wave eigenmodes in toroidal plasmas

Liu Chen and C. Z. Cheng

Plasma Physics Laboratory, Princeton University, Princeton, New Jersey 08544
(Received 27 June 1979; accepted 8 August 1980)

The eigenmode equation describing ballooning drift waves in toroidal plasmas is investigated both analytically and numerically. Two branches of eigenmodes are identified. One is slab-like and the other is a new branch induced by finite toroidal coupling. The slab-like eigenmodes correspond to unbounded states and experience finite shear damping. The toroidicity-induced eigenmodes, however, can become local quasi-bounded states with negligible shear damping. Both branches of eigenmodes may exist simultaneously. The corresponding analytical theories are also presented.

I. INTRODUCTION

Recently, there has been active interest in the stability properties of drift-wave eigenmodes in sheared magnetic fields. A crucial point to realize in stability analysis is, in the presence of finite magnetic shear, drift-wave eigenmodes in slab geometries experience anti-well potential structures and, therefore, finite damping due to energy convecting away from the mode-rational surface. The existence of this shear-induced convective damping or, simply, shear damping was first pointed out by Pearlstein and Berk.[1] On the other hand, as first emphasized by Taylor,[2] the shear damping mechanism may be modified significantly in toroidal plasmas, such as tokamaks. The physical arguments are as follows: In toroidal geometries, the mode-rational surfaces corresponding to different poloidal mode numbers are closely packed. Due to toroidal effects, such as curvature drifts, the neighboring poloidal modes are coupled. The drift-wave eigenmode centered about one particular mode-rational surface will therefore be affected by the wave energies which convect away from the neighboring eigenmodes. In other words, toroidal-coupling effects can modify the anti-well potential structure and, thereby, the shear damping mechanism. Using a model toroidal-coupling term, Taylor, in fact, demonstrated that the shear damping could be nullified. In his analysis, Taylor first reduced the two-dimensional eigenmode equation to a one-dimensional one by employing a representation now widely-known as ballooning-mode representation,[3-9] since its rigorous formulation was first developed in works treating ideal magnetohydrodynamic ballooning modes with high toroidal mode numbers.[3-5] The resultant model one-dimensional eigenmode equation then became an ordinary differential-difference equation with the difference operator originating from the toroidal-coupling term. Taylor then made the so-called strong-coupling assumption which approximated the difference operator by a differential operator (see Sec. II), thereby, further reduced the equation to a readily soluble second-order ordinary differential equation. Taylor's analytical approach (i.e., ballooning-mode representation and strong-coupling assumption) was later adopted, independently, by Tang[10] and Horton *et al.*,[11] to investigate a rigorously derived eigenmode equation for drift waves in an axisymmetric, large-aspect-ratio tokamak with concentric, circular magnetic surfaces where toroidal coupling appeared due to ion ∇B and curvature drifts. Their results indicate that nullification of shear damping only occurs when the shear is weak; $\hat{s} = rq'/q < \frac{1}{2}$. Here, $q = rB_t/RB_\theta$ is the usual safety factor of a tokamak. In fact, for normal tokamak shear $\hat{s} > \frac{1}{2}$, their results predict that shear damping is further enhanced by toroidal coupling. The validity regime of the strong-coupling assumption, however, can be shown to be rather restrictive; i.e., generally, it is valid only for rather weak toroidal coupling. We are, thus, motivated to examine this problem without making the strong-coupling assumption. That is, for normal tokamak parameters, we find drift-wave eigenmodes with negligible shear damping do exist even if the shear is strong ($\hat{s} > \frac{1}{2}$). Furthermore, we find that these quasi-marginally stable eigenmodes are associated with a new eigenmode branch which is induced entirely by toroidal coupling; that is, this (toroidicity-induced) eigenmode branch cannot be regarded as a continuation of the slab (Pearlstein-Berk) eigenmode branch into a toroidal plasma. In this respect, our results also differ from those obtained in two recent works,[7,8] where the quasi-marginally stable eigenmodes are shown to be smoothly connected to the slab eigenmodes. While we do not have an exact explanation for this difference, a plausible explanation may lie in the different numerical schemes employed to solve the eigenmode equation. Since the eigenmodes are damped and, therefore, diverge asymptotically along the real axis (see Sec. III), it becomes difficult to apply the numerical shooting scheme along the real axis and, in fact, results thus obtained could be erroneous. In the present work, we avoid this numerical difficulty by employing the interactive WKB-shooting code developed by White.[12] In this code, one first uses the Stokes' diagram to locate the subdominant regions in the complex plane, where the solutions decay asymptotically. Numerical shooting is then performed along an axis which ends inside the subdominant regions. Employing this scheme, not only the numerical difficulty disappears, but one can also readily perform the relevant phase integral to identify the quantization number of the eigenmode.

The theoretical model and the corresponding drift-ballooning eigenmode equation are given in Sec. II. In Sec. III, we discuss the relevant boundary conditions. Applying these boundary conditions, the eigenmode equation is solved numerically using the interactive WKB-shooting scheme and the results are presented in Sec. IV. The corresponding analytical theories are des-

 0031-9171/80/112242-08$00.90

cribed in Sec.V. Final conclusions and a discussion are given in Sec. VI.

II. THEORETICAL MODEL AND EIGENMODE EQUATION

Let us consider electrostatic drift waves in an axisymmetric, large-aspect-ratio torus with concentric, circular magnetic surfaces. We adopt the usual (r, θ, ξ) coordinates corresponding, respectively, to the (minor) radial, poloidal, and toroidal directions. The perturbed potential ϕ can be expressed as

$$\phi(r,\theta,\xi)=\sum_j \hat{\phi}_j(s)\exp[i(m_0\theta+j\theta-n\xi-\omega t)], \tag{1}$$

where $|j| \ll m_0$, $s=(r-r_0)/\Delta r_s$, r_0 is the reference mode-rational surface $m_0=nq(r_0)$, $\Delta r_s=1/k_\theta s$, $k_\theta=m_0/r_0$, and $\hat{s}=rq'/q$ at $r=r_0$. Following standard procedures (see Ref. 10), the two-dimensional eigenmode equation can be derived straightforwardly and is given by[7,10,11]

$$[L(s,j)+Q_1(s,j)-\epsilon_n T/\Omega]\hat{\phi}_j(s)=0\ , \tag{2}$$

$$L=b_\theta(\hat{s}^2 d^2/ds^2-1)\ , \tag{3}$$

$$Q_1=1/\Omega-1+[(s-j)/\eta_s\Omega]^2\ , \tag{4}$$

and

$$T\hat{\phi}_j(s)=\hat{\phi}_{j+1}(s)+\hat{\phi}_{j-1}(s)+\hat{s}\frac{\partial}{\partial s}[\hat{\phi}_{j+1}(s)-\hat{\phi}_{j-1}(s)]. \tag{5}$$

Here, $b_\theta=k_\theta^2\rho_s^2$, $\rho_s=c_s/\omega_{ci}$, $c_s=(T_e/M_i)^{1/2}$, $\Omega=\omega/\omega_{*e}$, $\eta_s=qb_\theta^{1/2}/\epsilon_n$, $\epsilon_n=r_n/R$, $r_n^{-1}=|d\ln N/dr|$, $\omega_{*e}=b_\theta^{1/2}c_s/r_n$, and R is the major radius. In deriving Eqs. (2)–(5), we have assumed $\tau=T_e/T_i \gg 1$ and made the small ion Larmor radius as well as fluid ion approximations. Furthermore, we have only kept the adiabatic electron response and ignored any electron destabilizing, temperature gradient, or trapped particle effects. We note that T, as defined in Eq. (5), is the toroidal-coupling operator due to ion ∇B and curvature drifts. We remark that we have suppressed the destabilizing effects here in order to concentrate on the shear damping mechanism in toroidal plasmas. However, it needs to be emphasized that (as stability analyses in slab geometries have clearly indicated) modifications in the shear damping mechanism will have a direct implication on the stability properties.

Since, typically, $|m_0| \sim |n| \sim |r_n/\rho_s| \sim 0(10^2\text{–}10^3)$, we may adopt the large-n ballooning-mode formalism.[3–8] In zeroth order, we have, with $z=s-j$, $\hat{\phi}_j(s)=\Phi(z)$ and $\hat{\phi}_{j\pm1}(s)=\Phi(z\mp1)$; i.e., the eigenmodes are composed of identical structures centered at each mode-rational surface. Equation (2) then reduces to a one-dimensional differential-difference equation; i.e.,

$$[L_1+Q_1(z)-\epsilon_n T_1/\Omega]\Phi(z)=0\ , \tag{6}$$

where

$$L_1=b_\theta(\hat{s}^2 d^2/dz^2-1),\quad Q_1(z)=1/\Omega-1+z^2/\Omega^2\eta_s^2\ ,$$

and

$$T_1\Phi=\Phi(z+1)+\Phi(z-1)+\hat{s}\frac{d}{dz}[\Phi(z-1)-\Phi(z+1)]. \tag{7}$$

Fourier transforming Eq. (6), we then obtain

$$[d^2/d\eta^2+\eta_s^2\Omega^2 Q(\Omega,\eta)]\hat{\phi}(\eta)=0;\quad -\infty<\eta<\infty\ , \tag{8}$$

where

$$Q(\Omega,\eta)=b_\theta(1+\hat{s}^2\eta^2)+1-1/\Omega+(2\epsilon_n/\Omega)(\cos\eta+\hat{s}\eta\sin\eta)\ , \tag{9}$$

and η can be regarded as the coordinate along the field lines.[3–8] Equation (8) is the drift-ballooning eigenmode equation to be analyzed. We note that Eq. (8) corresponds to perturbations centered at the outside of the torus and is similar to the equations derived by other authors.[6–8,10,11] Equation (9) shows that toroidal-coupling effects introduce modulations on the otherwise anti-well potential structures. We note that the strong-coupling assumption, which approximates T_1 as $T_1\Phi \simeq [2+(1-2\hat{s})d^2/dz^2]\Phi(z)$, is equivalent to expanding $Q(\Omega,\eta)$ about $\eta=0$ to $0(\eta^2)$. Thus, this assumption only considers eigenmodes highly localized about $\eta=0$ and, therefore, is rather restrictive. Before proceeding with the solution of Eq. (8), however, we need to discuss the relevant boundary conditions.

III. BOUNDARY CONDITIONS

As $|\eta|\to\infty$, $Q\to b_\theta\hat{s}^2\eta^2$, and for $\hat{\phi}=\exp(\pm i\int^\eta k_\eta d\eta)$, we have

$$k_\eta\to\Omega\eta_s b_\theta^{1/2}\hat{s}\eta\ , \tag{10}$$

or

$$\hat{\phi}\to\exp(\pm i\Omega\eta_s b_\theta^{1/2}\hat{s}\eta^2/2)\ . \tag{11}$$

For unstable eigenmodes (Im $\Omega>0$), that $\hat{\phi}$ must be spatially decaying requires us to take the plus sign; i.e.,

$$\hat{\phi}\to\exp(i\Omega\eta_s b_\theta^{1/2}\hat{s}\eta^2/2)\ . \tag{12}$$

Noting that

$$\partial\Omega/\partial k_\eta\to(\eta_s b_\theta^{1/2}\hat{s}\eta)^{-1}\ , \tag{13}$$

the boundary condition, as given by Eq. (12), then corresponds to outward wave energy propagation. On the other hand, there is difficulty in applying the outgoing-wave boundary condition, Eq. (12), to the marginally stable and damped eigenmodes (Im $\Omega\leq0$), which will not asymptotically decay. This difficulty, however, can be readily resolved by noting that, in the original configuration (z) coordinate, the outgoing-wave boundary condition is equivalent to the asymptotically decaying condition if the linear ion Landau damping term is included.[1] One would, therefore, expect similar properties in the Fourier transformed η coordinate.[7]

Retaining the ion Landau damping term, it is easy to show that the potential structure Q is modified to be

$$Q=Q+i\tau\sqrt{\pi}\,\xi_i\,\exp(-\xi_i^2)\ , \tag{14}$$

where ξ_i is an operator, $\xi_i = (\tau/2)^{1/2}\,\eta_s\Omega/|id/d\eta|$, and we have assumed $|\xi_i| > 1$ in deriving Eq. (14). Since $|\xi_i| > 1$, we may treat the ion Landau damping term perturbatively. Thus, as $|\eta| \to \infty$, the WKB wavenumber becomes

$$\tilde{k}_\eta \to k_\eta [1 + i\tau\sqrt{\pi}\,\xi_i \exp(-\xi_i^2)/2b_\theta \hat{s}^2\eta^2], \tag{15}$$

where k_η is given by Eq. (10) and

$$\xi_i = (\tau/2)^{1/2}\eta_s\Omega/|k_\eta| \to (\tau/2b_\theta)^{1/2}/\hat{s}|\eta| \ . \tag{16}$$

Meanwhile, we have

$$\hat{\phi}(\eta) \to \exp(\pm i\int^\eta k_\eta\, d\eta). \tag{17}$$

Since $\xi_i > 0$, the requirement that the solutions decay asymptotically, again, leads us to take the plus sign, i.e., the outgoing-wave boundary condition, Eq. (12). Indeed, from Eqs. (15) and (16), we note that even in the η coordinate the boundary condition, Eq. (12), describes the wave energy being propagated outward and absorbed by ion Landau damping at $|\eta| = \pm\infty$. Thus, Eq. (12) dictates that for damped eigenmodes ($\mathrm{Im}\Omega < 0$) the solutions be asymptotically divergent. With the appropriate boundary conditions determined, the eigenvalue problem as posed by Eq. (8) is thus completely specified.

IV. NUMERICAL RESULTS

In this section, we present the numerical results of eigenmode analyses using the interactive WKB-shooting code developed by White.[12] Detailed descriptions for this code are given in Ref. 12 and will not be repeated here.

In the present work, we have found that there exist two branches of eigenmodes. One is slab-like; i.e., this branch represents the continuation of the slab eigenmodes into the toroidal geometries. The other branch of eigenmodes is induced by the finite toroidal coupling; i.e., it has no counterpart in the slab limit and, in this sense, is a new (toroidicity-induced) branch of eigenmodes. In order to better understand the qualitative differences between the two eigenmode branches, it is helpful to examine the corresponding Stokes' diagrams, potential structures $-Q_r(\Omega, \eta_r)$ and eigenfunctions $\hat{\phi}(\eta_r)$; which are shown in Figs. 1 to 4. Figure 1 shows those for slab-like eigenmodes. We note that the complete Stokes' structure is rather complicated and, therefore, only three relevant pairs of turning points and associated anti-Stokes' lines are shown. Referring to Fig. 1(a), $\pm P$ correspond to the slab (Pearlstein-Berk)-like turning points (i.e., they exist even if toroidal coupling is absent); meanwhile, $\pm T_1$ and $\pm T_2$ correspond to turning points induced by the finite toroidal coupling. As shown in Fig. 1(b), the potential structure is an anti-well. The wave energy, therefore, can freely convect outward and the eigenmodes are damped. The boundary condition, Eq. (12), thus dictates that regions (i) and (i)′ be dominant and, hence, regions (ii) and (ii)′ be subdominant. The corresponding WKB eigenvalue condition is then determined by the slab-like turning

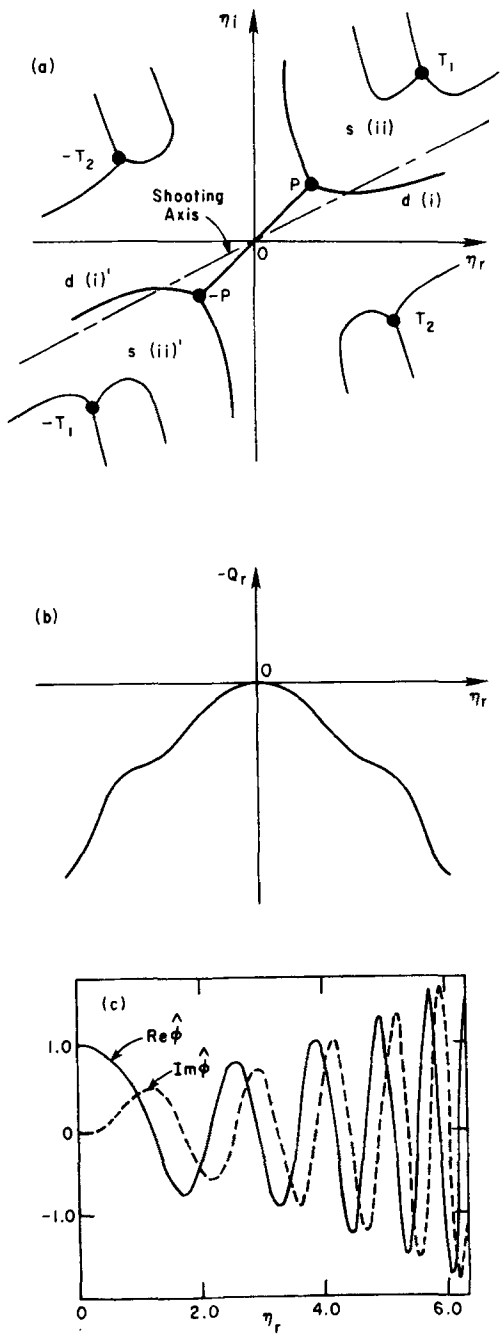

FIG. 1. Typical (a) anti-Stokes' plot, (b) potential structure, and (c) eigenfunction for the slab-like eigenmode branch. $\pm P$, $\pm T_1$, and $\pm T_2$ correspond to turning points in the complex η plane. s and d denote, respectively, subdominant and dominant regions.

points, $\pm P$; i.e.,

$$\Omega\eta_s\int_{-P}^{P} Q^{1/2}\,d\eta = \left(n + \frac{1}{2}\right)\pi, \quad n = 0, 1, \ldots, \tag{18}$$

and, therefore, the eigenmodes are called slab-like eigenmodes. We note that Eq. (18) is useful not only in identifying the quantization number of the eigenmode, but also in tracking its evolution as the physical parameters change. In Fig. 1(a), we also indicate the axis in the complex plane along which the numerical shooting is done. Using the obtained eigenvalue Ω, we can then plot the eigenfunction along the real η axis $\hat{\phi}(\eta_r)$, as shown

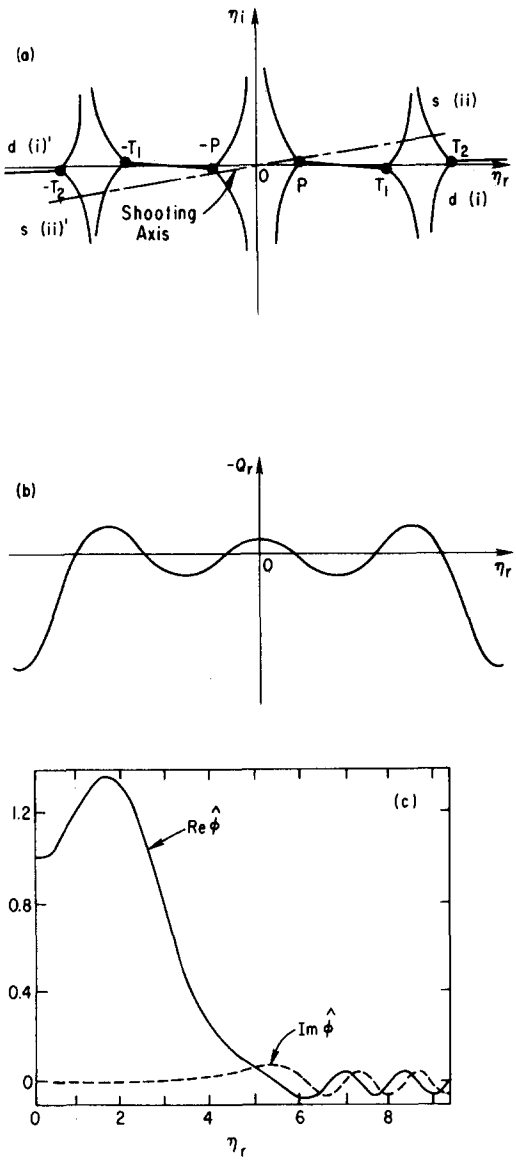

FIG. 2. Typical (a) anti-Stokes' plot, (b) potential structure, and (c) eigenfunction for the weak toroidicity-induced eigenmode branch. The rest is the same as Fig. 1.

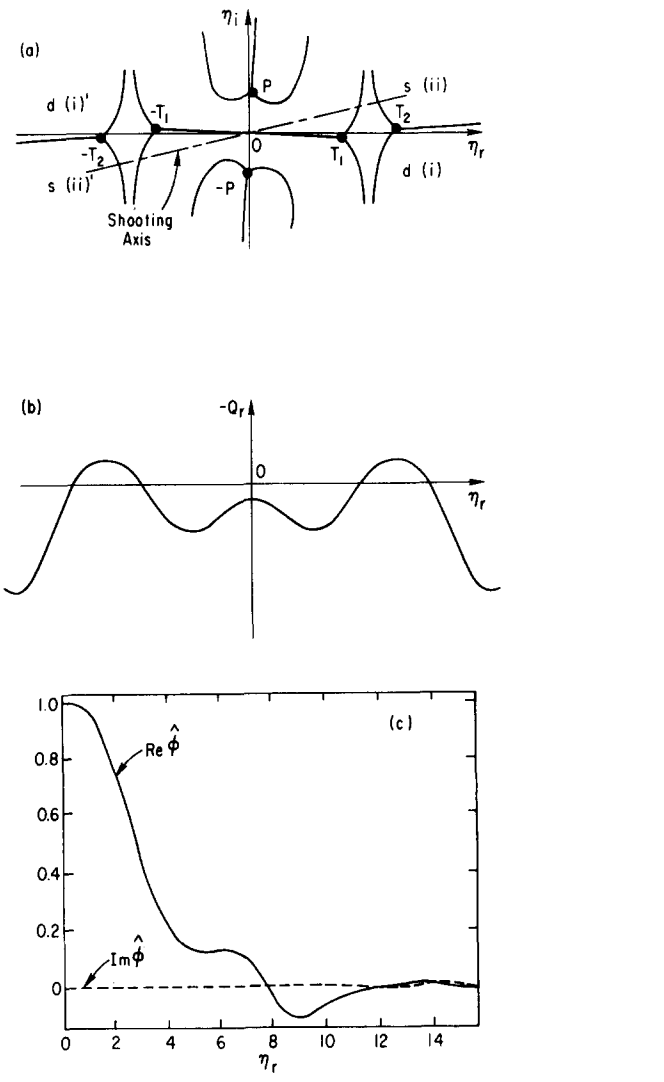

FIG. 3. Typical (a) anti-Stokes' plot, (b) potential structure, and (c) eigenfunction for the strong toroidicity-induced eigenmode branch with $\hat{s} = rq'/q > \frac{1}{2}$. The rest is the same as Fig. 1.

in Fig. 1(c) for the $n = 0$ eigenstate, which clearly exhibits the asymptotically divergent behavior.

As to the toroidicity-induced eigenmodes, their properties depend on the shear strength $\hat{s}$ and the toroidicity ϵ_n. Three cases have been identified: (i) $\hat{s} > \frac{1}{2}$ and small ϵ_n, (ii) $\hat{s} > \frac{1}{2}$ and large ϵ_n, and (iii) $\hat{s} < \frac{1}{2}$. The corresponding Stokes' diagrams, potential structures, and eigenfunctions are sketched in Figs. 2, 3, and 4, respectively. Note that only those eigenmodes which are quasi-marginally stable are illustrated. Since, as ϵ_n is increased, case (i) evolves into case (ii), we classify case (i) and case (ii) as the weak and strong toroidicity-induced eigenmodes, respectively. Case (iii) is also classified as a strong toroidicity-induced eigenmode because its Stokes' diagram is similar to that of case (ii). From Figs. 2–4 it is clear that these quasi-marginally stable toroidicity-induced eigenmodes are characterized by eigenstates bounded by local potential wells, which may be localized either about or away from $\eta = 0$. Contrary to the slab-like branch with anti-well potentials, the outward convection of the wave energy occurs here only through the tunneling leakage; therefore, we may expect the shear damping rates to be significantly reduced. In this respect, we can regard these eigenmodes as quasi-bounded states which are quasi-marginally stable. The plots of eigenfunctions, Figs. 2(c) and 3(c) further demonstrate the quasi-bounded nature of the eigenmodes. Referring to Figs.

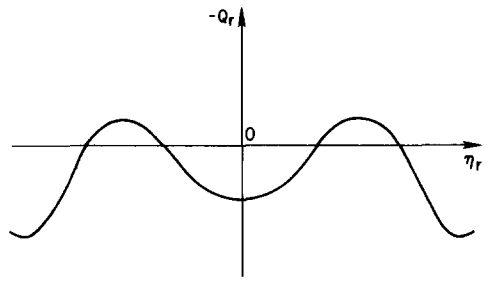

FIG. 4. Typical potential structure for the strong toroidicity-induced eigenmode with $\hat{s} < \frac{1}{2}$. The anti-Stokes' plot and eigenfunction are similar to those in Fig. 3.

2(a) and 3(a), the WKB eigenvalue conditions for the weak and strong toroidicity-induced eigenmodes are, respectively,

$$\Omega\eta_s\int_P^{T_1} Q^{1/2}d\eta=\left(n+\frac{1}{2}\right)\pi+\delta_1\ , \tag{19}$$

and

$$\Omega\eta_s\int_{-T_1}^{T_1} Q^{1/2}d\eta=\left(n+\frac{1}{2}\right)\pi+\delta_2;\quad \text{for } n=0,\ 1,\ldots, \tag{20}$$

where δ_1 and δ_2 correspond to tunneling leakage. Equations (19) and (20) indicate that the toroidicity-induced turning points, $\pm T_1$ and $\pm T_2$, play rather crucial roles in this eigenmode branch and, thus, we identify it as the toroidicity-induced eigenmode branch. While so far we have only discussed the quasi-marginally stable eigenmodes, we note that cases (i) and (ii) also possess damped eigenmodes with the turning points, $\pm P$, $\pm T_1$, and $\pm T_2$, located appreciably away from the η_r axis. The WKB eigenvalue conditions remain essentially the same as those given by Eqs. (19) and (20) and can be used to identify these damped eigenmodes as the higher-n eigenstates of the toroidicity-induced branch. The corresponding potential structures and eigenfunctions, however, look very similar to those of the slab-like branch. This further illustrates the desirability of using the Stokes' diagrams to identify the eigenmode branch.

We have examined the evolution of the two branches of eigenmodes as the parameters $\hat{s}$ and ϵ_n are varied. Only the $n=0$ eigenstate, which is the least shear damped, is studied here. In the following results, we have fixed $b_\theta=0.1$ and $q=1$. Figures 5 and 6 plot the eigenfrequencies $\Omega=\Omega_r+i\Omega_i$ vs ϵ_n for $\hat{s}=1$, and 0.3, respectively. For comparison, we also show the shear-damping rates in the slab approximation (i.e., without the toroidal-coupling term) $\Omega_i=-\hat{s}\epsilon_n/q(1+b_\theta)$. Figure 5 shows that for $\hat{s}=1$ both eigenmode branches can exist simultaneously. It is interesting to note that, as

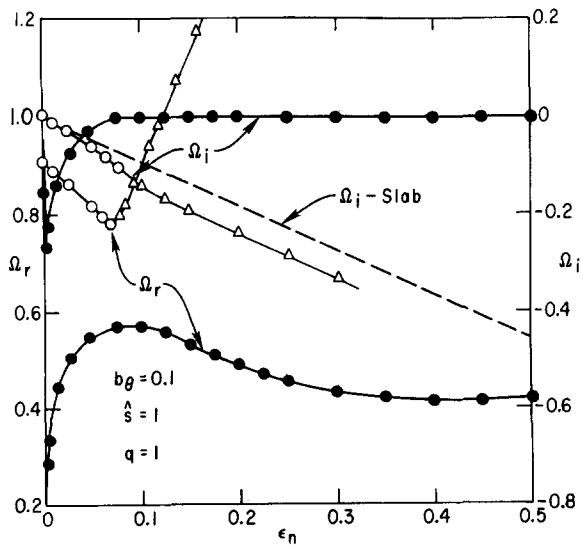

FIG. 5. Plot of eigenmode frequencies Ω vs ϵ_n for $b_\theta=0.1$, $q=1$, and $\hat{s}=1$. ○, ● and △ correspond, respectively, to the $n=0$ slab-like, $n=0$ and $n>0$ toroidicity-induced eigenmodes.

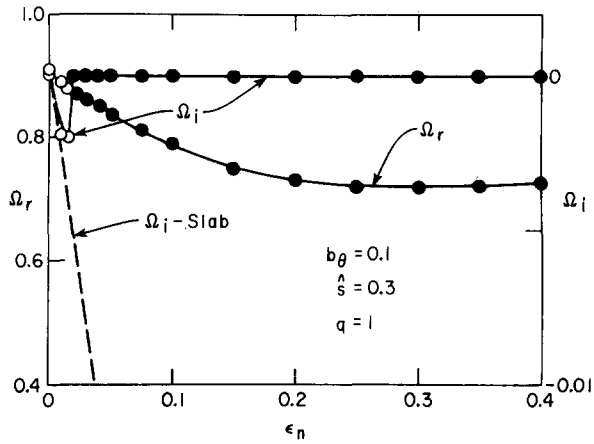

FIG. 6. Same as Fig. 5, except $\hat{s}=0.3$.

$\epsilon_n\to 0$, Ω (slab-like) $\to 1/(1+b_\theta)$ (i.e., the local dispersion relation); meanwhile, Ω(toroidicity-induced) $\to 0$. That the two limiting behaviors are qualitatively different further supports the observation that these are two distinctive eigenmode branches. As ϵ_n increases, the damped slab-like eigenmode evolves into a damped toroidicity-induced eigenmode at $\epsilon_n\simeq 0.075$. Meanwhile, the corresponding shear-damping rate is larger than that in the slab approximation. On the other hand, the damped weak toroidicity-induced eigenmode at small ϵ_n becomes quasi-marginally stable at $\epsilon_n\simeq 0.075$ and, as ϵ_n is further increased, evolves into a strong toroidicity-induced eigenmode at $\epsilon_n\simeq 0.2$. At quasi-marginal stability, the shear-damping rate is negligibly small; typically, $|\Omega_i|\sim 0(10^{-3}-10^{-4})$.

In the weak shear ($\hat{s}=0.3$) case, Fig. 6 shows that the damped slab-like branch, which exists for $\epsilon_n<0.02$, is connected to the strong toroidicity-induced branch, which is quasi-marginally stable. Thus, in this case, there exists only a single branch of eigenmodes for a value of ϵ_n. Meanwhile, contrary to the $\hat{s}=1$ case, the shear-damping rates of the slab-like branch are somewhat reduced by the toroidicity.

Figure 7 shows the dependence of the eigenmodes on the shear strength $\hat{s}$ for a fixed $\epsilon_n=0.1$. The slab-like eigenmode now exists for large $\hat{s}$ and, as $\hat{s}$ is reduced, is connected to a damped toroidicity-induced eigenmode at $\hat{s}\simeq 2$. In this respect, its dependence on $\hat{s}$ is reversed to that on ϵ_n. Again, the damping rate is larger than that in the slab approximation. As to the toroidicity-induced eigenmode, it is interesting to note that a quasi-marginally stable eigenmode exists even at large $\hat{s}$. As $\hat{s}$ is reduced, the eigenmode evolves from a weak toroidicity-induced to a strong toroidicity-induced eigenmode at $\hat{s}\simeq 0.6$. The damping rate, meanwhile, is negligibly small for the entire range of $\hat{s}$.

In the following, we summarize the numerical results:

(1) There exist two distinctive eigenmode branches, one is the slab-like and the other is toroidicity-induced.

(2) For normal shear $\hat{s}>\frac{1}{2}$, the two branches can exist simultaneously. For weak shear $\hat{s}<\frac{1}{2}$, however, they are connected.

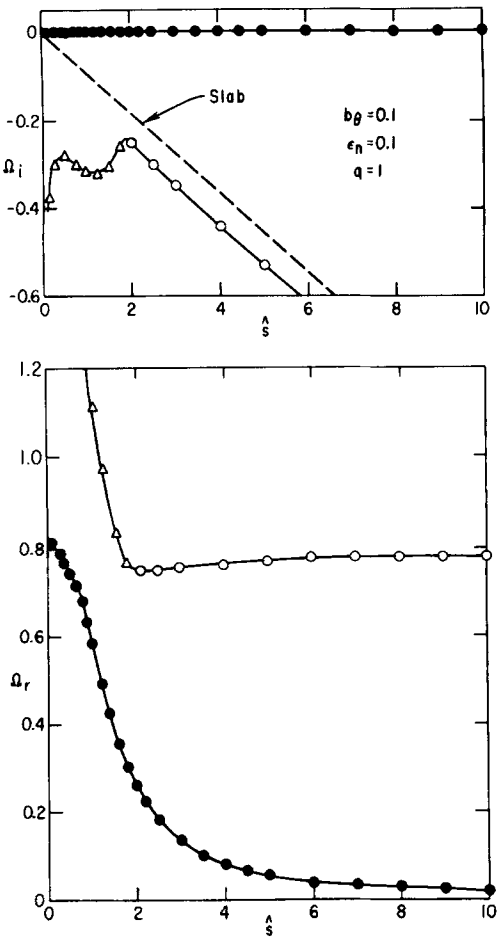

FIG. 7. Plot of Ω vs $\hat{s}$ for $b_\theta = 0.1$, $q = 1$, and $\epsilon_n = 0.1$. The other notations are the same as Fig. 5.

(3) The damped slab-like eigenmode exists when either, with $\hat{s}$ fixed, $\epsilon_n < \epsilon_{cs}$ or, with ϵ_n fixed, $\hat{s} > \hat{s}_{cs}$. For normal (weak) shear, the shear-damping rate is further enhanced (reduced) by the toroidal-coupling effects.

(4) For normal (weak) shear, the slab-like eigenmode is connected with a damped (quasi-marginally stable) toroidicity-induced eigenmode. The damped eigenmode, again, has an enhanced shear-damping rate.

(5) For fixed normal shear, the toroidicity-induced branch becomes quasi-marginally stable when $\epsilon_n > \epsilon_{cT}$ and can remain so even for $\hat{s} \gg 1$. For $\epsilon_n < \epsilon_{cT}$, it is damped and, furthermore, $\Omega \to 0$ as $\epsilon_n \to 0$.

The results described in this section provide useful insights in developing analytical theories, which, in turn, not only explain these results but also, more importantly, generalize the results to a wider parameter space.

V. ANALYTICAL THEORIES

A. Slab-like eigenmodes

For this branch of eigenmodes, the complex turning points are located near $\eta = 0$; i.e., $|P| < 1$ (cf. Fig. 1). Therefore, we may assume $|\eta| < 1$ and approximate Q as

$$Q(\Omega, \eta) \simeq Q(\Omega, 0) + Q''(\Omega, 0)\eta^2/2 , \tag{21}$$

where

$$Q(\Omega, 0) = 1 + b_\theta - 1/\Omega + 2\epsilon_n/\Omega , \tag{22}$$

and

$$Q''(\Omega, 0) = 2[b_\theta \hat{s}^2 + \epsilon_n(2\hat{s} - 1)/\Omega] . \tag{23}$$

Equation (8) then becomes a standard Weber's equation and can readily be solved. Applying the outgoing-wave boundary condition, we obtain the following dispersion relations[10, 11]

$$\Omega = \frac{1 - 2\epsilon_n}{1 + b_\theta} - i\,\frac{(2n+1)\epsilon_n}{q(1+b_\theta)}\left(\hat{s}^2 + \frac{\epsilon_n(2\hat{s}-1)}{b_\theta \Omega}\right)^{1/2} ;$$

$$n = 0, 1, \cdots . \tag{24}$$

Since $\Omega > 0$, Eq. (24) clearly shows that for $\hat{s} > \frac{1}{2}$ ($\hat{s} < \frac{1}{2}$), the shear damping is further enhanced (reduced) by toroidal coupling. We note that assumption $|P| < 1$ is identical to the strong-coupling assumption. Furthermore, while the eigenmodes are localized about $\eta = 0$ in the complex plane, they are extended along the η_r coordinate.

For $\hat{s} < \frac{1}{2}$, the slab-like branch disappears when the anti-well potential structure about $\eta = 0$ is absent; i.e., $Q''(\Omega, 0) = 0$. From Eqs. (23) and (24), we obtain the critical value of ϵ_n, ϵ_{cs1}, as

$$\epsilon_{cs1} \simeq b_\theta \hat{s}^2/[(1 + b_\theta)(1 - 2\hat{s}) + 2b_\theta \hat{s}^2] . \tag{25}$$

For $b_\theta = 0.1$ and $\hat{s} = 0.3$, we find $\epsilon_{cs1} = 0.02$ in agreement with the numerical result (cf., Fig. 6). For $\hat{s} > \frac{1}{2}$, however, $Q''(\Omega, 0)$ never vanishes and the slab-like eigenmode evolves into a damped toroidicity-induced eigenmode when the strong-coupling assumption ($|P| < 1$) breaks down at $\epsilon_n = \epsilon_{cs2}$, which is approximately given by

$$\epsilon_{cs2} = q^2 b_\theta \alpha/(1 + b_\theta + 2q^2 b_\theta \alpha) , \tag{26}$$

with $\alpha = \hat{s} - \frac{1}{2} + \frac{1}{2}[(2\hat{s} - 1)^2 + (2\hat{s}/q)^2]^{1/2}$. For $\hat{s} = 1$ and $b_\theta = 0.1$, we find $\epsilon_{cs2} \simeq 0.1$ which agrees reasonably well with the numerical result shown in Fig. 5.

B. Toroidicity-induced eigenmodes

The numerical results described in Sec. IV indicate that this eigenmode branch becomes quasi-marginally stable when $\epsilon_n \geq \epsilon_{cT}$. For $\hat{s} < \frac{1}{2}$, we have $\epsilon_{cs1} = \epsilon_{cT1}$ given by Eq. (25). In the following, we shall derive the analytical expression of ϵ_{cT} for $\hat{s} > \frac{1}{2}$. At $\epsilon_n = \epsilon_{cT2}$, the corresponding potential structure, $-Q_r(\Omega, \eta_r)$, is shown in

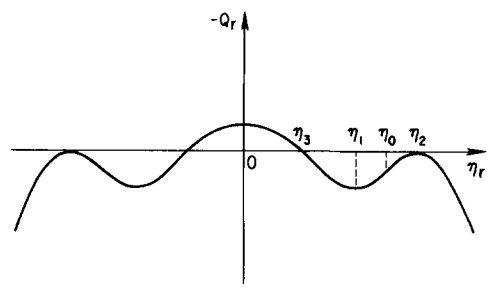

FIG. 8. Potential structure for $\epsilon_n = \epsilon_{cT2}$, where the weak toroidicity-induced eigenmode becomes quasi-marginally stable.

Fig. 8. From Fig. 8, we have the following five conditions:

$$Q_r(\Omega, \eta_2) = 0 , \tag{27}$$

$$Q_r'(\Omega, \eta_2) = 0 , \tag{28}$$

$$Q_r'(\Omega, \eta_1) = 0 , \tag{29}$$

$$Q_r(\Omega, \eta_3) = 0 , \tag{30}$$

and

$$\Omega\eta_s \int_{\eta_3}^{\eta_2} Q^{1/2} d\eta = \left(n + \frac{1}{2}\right)\pi, \quad n = 0, 1, \ldots \tag{31}$$

for the five unknowns; η_1, η_2, η_3, ϵ_{cT2}, and $\Omega = \Omega_c$. Note in Eq. (31), that we have neglected the tunneling leakage and, therefore, Ω_c is purely real. Since analytical expressions for Eq. (31) are generally difficult to obtain, we approximate the potential well about η_1 to be parabolic. Thus, as a replacement for Eqs. (30) and (31), we have, for the $n = 0$ eigenstate, the condition

$$Q_r(\Omega_c, \eta_1) = [-Q_r''(\Omega_c, \eta_1)/b_\theta]^{1/2}(\epsilon_{cT2}/q\Omega_c) . \tag{32}$$

To make further analytical progress, we shall solve Eqs. (27), (28), (29), and (32) by successive approximations; that is, we assume η_1 and η_2 are sufficiently close to η_0, where $Q_r''(\eta_0) = 0$. We thus, let $\eta_1 = \eta_0 - \delta_1$ and $\eta_2 = \eta_0 + \delta_2$ with δ_1, $\delta_2 < 1$. Correspondingly, we let $\epsilon_{cT2} = \epsilon_0 + \epsilon_1$ and $\Omega_c = \Omega_0 + \Omega_1$, such that $|\epsilon_1/\epsilon_0|$, $|\Omega_1/\Omega_0| < 1$. Carrying out the straightforward algebra, we obtain

$$\epsilon_{cT2} = \epsilon_0\{1 + \beta^2[1 + 2\hat{s}(1 + \pi b_1\beta)\epsilon_0]\}, \tag{33}$$

where

$$\epsilon_0 = b_\theta \hat{s}/[1 + b_\theta(1 + \hat{s}^2\pi^2 - 2\hat{s}^2)], \tag{34}$$

$\beta = (a_1/8\pi q^2 b_1)^{1/5}$, $b_1 = (2/a_1)^{1/2}$, and $a_1 = 1 + (\hat{s} - 1)(4\hat{s} - 1)/\hat{s}^2\pi^2$. An interesting property predicted by this analytical theory is, as either $b_\theta \to \infty$ or $\hat{s} \to \infty$, we have

$$\epsilon_{cT2} \to (1 + d_1)d_0/\hat{s} \equiv \bar{\epsilon}_c , \tag{35}$$

where $d_0 = 1(\pi^2 - 2 + \hat{s}^{-2})$ and $d_1 = \beta^2[1 + 2(1 + \pi b_1\beta)d_0]$. That is, there exists a maximum value of ϵ_{cT2}, $\bar{\epsilon}_c$, which is a constant for a fixed $\hat{s}$. This predicted property is consistent with the numerical result that the toroidicity-induced branch remains quasi-marginally stable for $\hat{s} \gg 1$. For $q = \hat{s} = 1$, in Fig. 9 we have plotted the analytically predicted ϵ_{cT2} vs b_θ. As can be seen, the analytical predictions agree rather well with the numerical results. Meanwhile, in this case, we find $\bar{\epsilon}_c \simeq 0.14$.

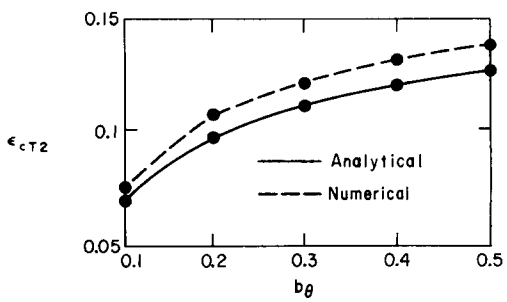

FIG. 9. Plots of ϵ_{cT2} vs b_θ for $q = \hat{s} = 1$.

Finally, we remark that, as $\epsilon_n \to 0$, the Stokes' diagram indicates that the turning-point pairs $\pm(P, T_1)$, while slowly migrating toward infinity in the complex plane, tend to coalesce toward each other. Using the coalescence condition $Q \simeq Q' \simeq 0$ plus $\mathrm{Im}\, P \simeq \mathrm{Im}\, T_1 \gg 1$, one can readily show the small ϵ_n behavior of Ω; particularly, $|\Omega| \to 0$ as $\epsilon_n \to 0$.

VI. CONCLUSIONS AND DISCUSSION

In this work, we have examined the shear damping of the drift-wave eigenmodes in toroidal plasmas. The toroidal-coupling effects considered here are due to the ion ∇B and curvature drifts. The corresponding drift-ballooning eigenmode equation, derived via the ballooning mode formalism, is then analyzed numerically using the WKB-shooting scheme. It is found that toroidal coupling introduces modulations to the potential structures. Two eigenmode branches are then found to exist. One is slab-like and the other is a new branch induced by the finite toroidal coupling. The slab-like eigenmode branch exists for small toroidicities and has anti-well potential structures. The eigenmodes, thus, correspond to unbounded states and experience finite shear damping. For $\hat{s} = rq'/q > \frac{1}{2}$, toroidal coupling further enhances the shear-damping rates. For $\hat{s} < \frac{1}{2}$, however, the shear-damping rates are somewhat reduced by the toroidal effects. On the other hand, the new (toroidicity-induced) eigenmode branch, which has no counterpart in the slab limit, can have eigenmodes which are quasi-bounded by local potential wells. Shear damping occurs only through tunneling leakage and is, generally, negligible. The quasi-bounded toroidicity-induced eigenmodes, therefore, can be regarded as quasi-marginally stable. For certain parameters, both eigenmode branches can exist simultaneously. We have also developed the corresponding analytical theories, which agree both qualitatively and quantatively with the numerical results. An interesting property predicted by the analytical theories is that quasi-marginally stable toroidicity-induced branch can exist even when b_θ, $\hat{s} \gg 1$ for reasonable toroidicities, i.e., $\epsilon_n \sim 0(10^{-1})$.

Since destabilizing effects, such as electron dissipation, are suppressed here in order to concentrate on the shear damping effects, this work, therefore, does not answer the stability question. However, some remarks may be made on the implication of the present results on the stability properties. Let us concentrate on the universal drift mode. In this case, electron dissipation can easily be incorporated into the one-dimensional differential-difference eigenmode equation, Eq. (6). As noted in Sec. V, we may apply the strong-coupling assumption for the slab-like branch. Equation (6) can then be reduced to a second-order differential equation and readily solved.[10, 11, 13] Generally speaking, the results show that unstable eigenmodes exist only for weak shear, i.e., $\hat{s} < \frac{1}{2}$. As for the quasi-marginally stable toroidicity-induced eigenmodes, it may be expected that finite electron dissipation can render the

eigenmodes absolutely unstable. This expectation, however, remains to be verified.

The existence of the toroidicity-induced eigenmode branch clearly indicates that, contrary to conventional thinking, toroidal-coupling effects cannot be simply regarded as (regular) perturbations to the slab eigenmode branch. In this respect, it is interesting to note the possibility that trapped particles can play not only the usual destabilizing role but also, through the associated toroidal-coupling effects, the new role of introducing new eigenmode branches.

Finally, we remark that the present analysis can easily be extended to consider perturbations which may be centered away from the outside of the torus.

ACKNOWLEDGMENTS

The authors acknowledge useful discussions with R. L. Dewar, E. A. Frieman, A. H. Glasser, P. K. Kaw, and R. B. White.

This work was supported by the United States Department of Energy Contract No. DE-AC02-76-CH-3-73.

[1]L. D. Pearlstein and H. L. Berk, Phys. Rev. Lett. **23**, 220 (1969).
[2]J. B. Taylor, in *Plasma Physics and Controlled Nuclear Fusion Research* (International Atomic Energy Agency, Vienna, 1977), Vol. II, p. 323.
[3]J. W. Connor, R. J. Hastie, and J. B. Taylor, Proc. R. Soc. **365**, 1 (1979).
[4]A. H. Glasser, in *Proceedings of the Finite Beta Theory Workshop*, Varenna, 1977, edited by B. Coppi and W. Sadowski (U.S. Department of Energy, CONF-7709167, 1977), p. 55. Also, R. L. Dewar, M. S. Chance, A. H. Glasser, J. M. Greene, and E. A. Frieman, Princeton Plasma Physics Laboratory Report PPPL-1587 (1979).
[5]Y. C. Lee and J. W. Van Dam, in *Proceedings of the Finite Beta Theory Workshop*, Varenna, 1977, edited by B. Coppi and W. Sadowski (U.S. Department of Energy, CONF-7709167, 1977), p. 93.
[6]E. A. Frieman, W. M. Tang, G. M. Rewoldt, and A. H. Glasser, Phys. Fluids **23**, 1750 (1980).
[7]R. J. Hastie, K. W. Hesketh, and J. B. Taylor, Nucl. Fusion, **19**, 1223 (1979).
[8]D. I. Choi and W. Horton, Phys. Fluids **23**, 356 (1980).
[9]K. T. Tsang and P. J. Catto, Phys. Rev. Lett. **39**, 1664 (1977).
[10]W. M. Tang, Nucl. Fusion **18**, 1089 (1978).
[11]W. Horton, Jr., R. D. Estes, H. Kawk, and D. I. Choi, Phys. Fluids **21**, 1366 (1978).
[12]R. B. White, J. Comput. Phys. **31**, 409 (1979).
[13]L. Chen, P. N. Guzdar, J. Y. Hsu, P. K. Kaw, C. R. Oberman, and R. B. White, Nucl. Fusion **19**, 373 (1979).